Macromolecules

Article

pubs.acs.org/Macromolecules

Thickness-Dependent Order-to-Order Transitions of Bolaform-like Giant Surfactant in Thin Films

Chih-Hao Hsu,[†] Kan Yue,[†] Jing Wang,[†] Xue-Hui Dong,[†] Yanfeng Xia,[‡] Zhang Jiang,[§] Edwin L. Thomas,*[,∥] and Stephen Z. D. Cheng*[,†]

[†]Department of Polymer Science, College of Polymer Science and Polymer Engineering, and [‡]Department of Polymer Engineering, College of Polymer Science and Polymer Engineering, The University of Akron, Akron, Ohio 44325, United States

[§]X-ray Science Division, Advanced Photon Source, Argonne National Laboratory, 9700 South Cass Avenue, Argonne, Illinois 60439, United States

[∥]Department of Materials Science and Nano Engineering and Department of Chemical and Biomolecular Engineering, Brown School of Engineering, Rice University, Houston, Texas 77251, United States

Supporting Information

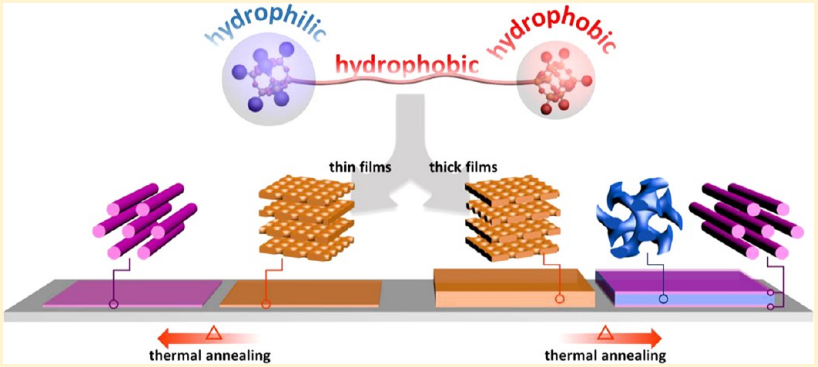

ABSTRACT: Controlling self-assembled nanostructures in thin films allows the bottom-up fabrication of ordered nanoscale patterns. Here we report the unique thickness-dependent phase behavior in thin films of a bolaform-like giant surfactant, which consists of butyl- and hydroxyl-functionalized polyhedral oligomeric silsesquioxane (BPOSS and DPOSS) cages telechelically located at the chain ends of a polystyrene (PS) chain with 28 repeating monomers on average. In the bulk, BPOSS-PS_{28}-DPOSS forms a double gyroid (DG) phase. Both grazing incidence small-angle X-ray scattering and transmission electron microscopy techniques are combined to elucidate the thin film structures. Interestingly, films with thicknesses thinner than 200 nm exhibit an irreversible phase transition from hexagonal perforated layer (HPL) to compressed hexagonally packed cylinders (c-HEX) at 130 °C, while films with thickness larger than 200 nm show an irreversible transition from HPL to DG at 200 °C. The thickness-controlled transition pathway suggests possibilities to obtain diverse patterns via thin film self-assembly.

INTRODUCTION

Utilizing self-assembly of soft materials to fabricate thin films or coatings with ordered patterns provides a bottom-up approach to overcome limitations in top-down approaches.[1−3] Among a variety of self-assembled ordered phases, e.g., lamellae (LAM), double gyroid (DG), hexagonally packed cylinders (HEX), and body-centered-cubic packed spheres (BCC), the three-dimensional (3D) DG phase attracts a great deal of scientific interest because its bicontinuous structure within a cubic lattice holds great potential in applications of self-supporting porous materials and 3D photonics.[4,5] Luzzati and Spegt[6] were the first to observe the DG phase having $Ia\bar{3}d$ symmetry in an anhydrous amphiphilic soap system. For block copolymers, the first experimental observation of the bicontinuous cubic phase was by Thomas et al.,[7] and the symmetry of $Ia\bar{3}d$ was determined afterward by the works of Gruner and Thomas et al.[8] and Bates et al.[9] Theoretical calculations have suggested that the DG phase is a thermodynamically equilibrium phase in the weak-to-intermediate segregation limit.[10,11] On the other hand, the hexagonal perforated layer (HPL) phase has been closely related to the DG phase, typically via an irreversible phase transition, as widely observed in diblock copolymer and diblock copolymer/homopolymer blend systems.[12−22] The HPL structure consists of alternative stacked layers of the major and minor components with hexagonally arranged perforations in the minor-component layers by the continuous major-component phase. The HPL phase is theoretically predicted to be a metastable phase[22−24] and has been experimentally observed as a long-live metastable structure, which could be induced by large-amplitude mechanical shear to

Received: July 25, 2017
Revised: September 1, 2017
Published: September 11, 2017

DOI: 10.1021/acs.macromol.7b01598
Macromolecules 2017, 50, 7282−7290

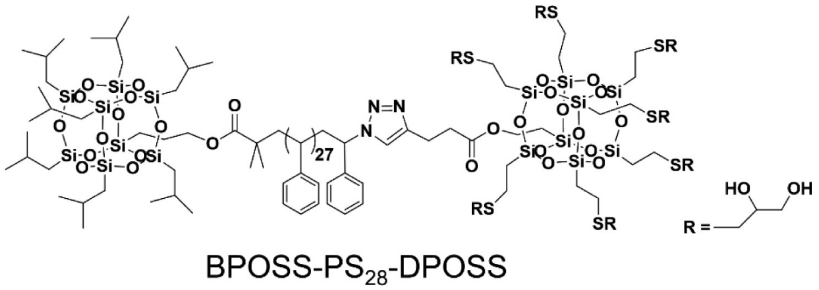

Figure 1. Molecular structure of BPOSS-PS_{28}-DPOSS. The volume fraction of each component is Φ_{BPOSS} = 0.19, Φ_{PS} = 0.59, and Φ_{DPOSS} = 0.22.

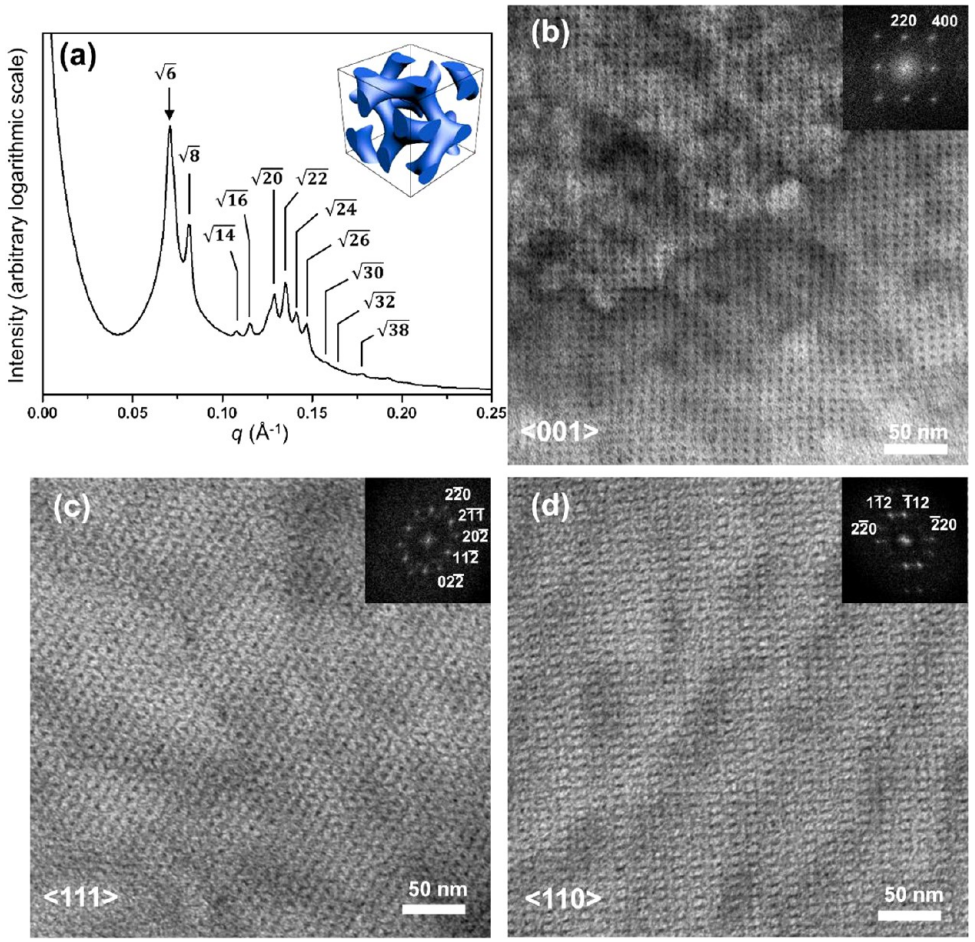

Figure 2. Structural characterizations of a bulk sample of BPOSS-PS_{28}-DPOSS. (a) 1D SAXS pattern of BPOSS-PS_{28}-DPOSS bulk sample after annealing at 120 °C for 2 h. A set of BF TEM images of the microtomed bulk sample showing projections of the structure along the (b) ⟨001⟩, (c) ⟨111⟩, and (d) ⟨110⟩ directions of the DG phase. In the BF TEM images, DPOSS domains are shown in dark and BPOSS/PS domains are shown in gray after the selective OsO_4 staining to the hydroxyl groups of DPOSS cages. The insets represent the corresponding FFT images with prominent Bragg peaks labeled.

create the edge dislocations and lower the energy barrier of forming the HPL phase compared to that of the DG phase.[20,22]

Although the phase behavior and the physical characterization of the DG phase in the bulk state have been studied extensively, studies on the DG phase in thin films[26−29] and the corresponding thickness-dependent phase behavior are relatively limited.[30] In the thin film state, the stability of a particular phase is influenced by additional factors including the geometric confinement and the interactions between films and surfaces, i.e., a surface field,[31−33] which are known to also affect the phase orientations.[34−36] In some cases, the confinement constraints present in thin films may even stabilize a metastable structure. Despite extensive interest in the DG and HPL phases, the thickness-dependent stability of these phases remains largely unexplored.

To address this question, we selected a DG-forming, bolaform-like giant surfactant and systematically investigated its thickness-dependent phase behavior. Giant surfactants, which consist of molecular nanoparticles (such as functionalized polyhedral oligomeric silsesquioxane (POSS) cages) tethered at the ends of polymer chains, bear structural similarities to both small-molecule surfactants and block copolymers.[37] In the bulk, a variety of ordered phases have been observed in a POSS−polystyrene (POSS−PS) giant

DOI: 10.1021/acs.macromol.7b01598
Macromolecules 2017, 50, 7282−7290

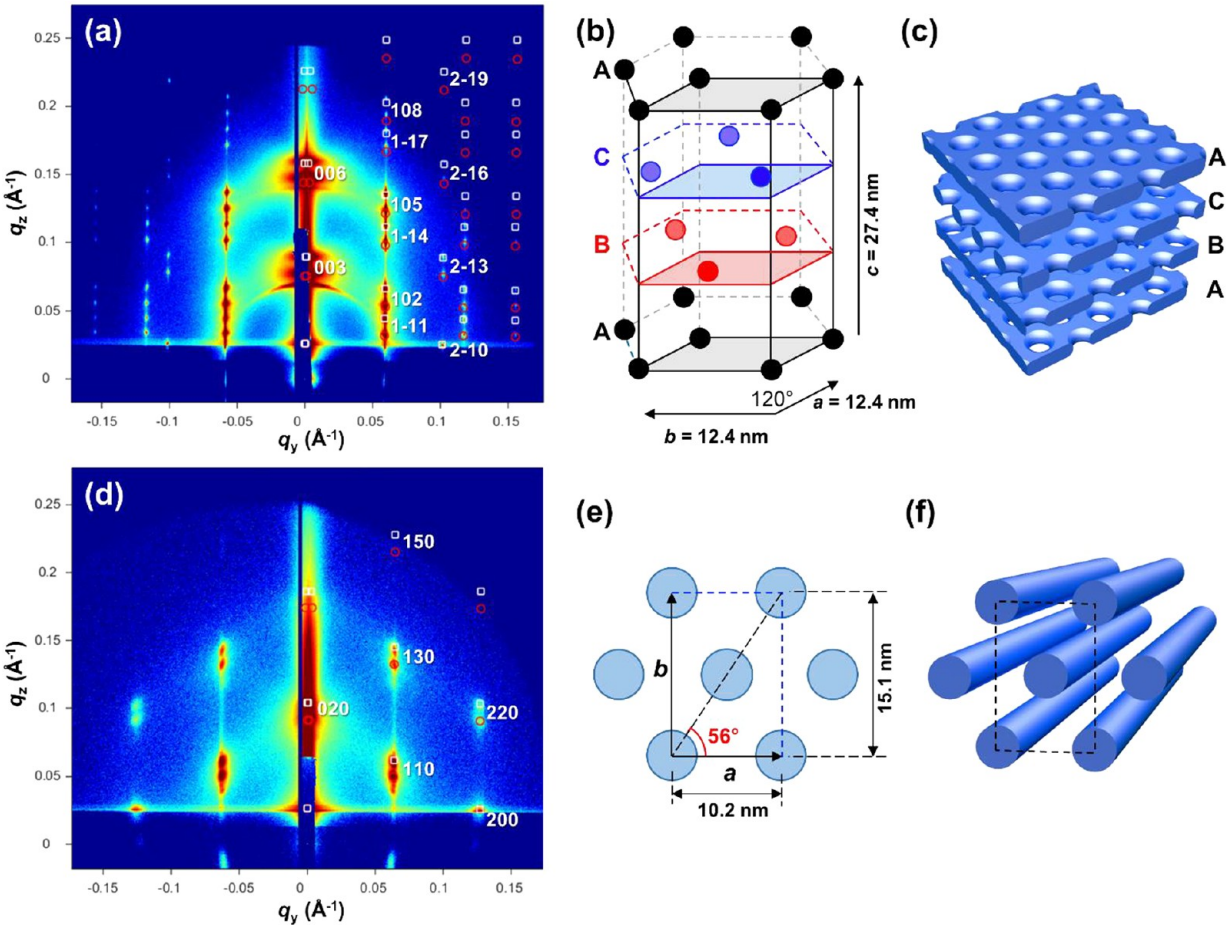

Figure 3. Structural characterizations of a 138 nm thick ($15L_0$) film of BPOSS-PS_{28}-DPOSS. (a) GISAXS pattern at the incident angle of 0.20° of the BPOSS-PS_{28}-DPOSS thin film after annealing at 120 °C for 4 days. The Miller indexes in the GISAXS pattern are based on (b) the hexagonal lattice of a HPL structure, which is equivalent to a trigonal lattice with $R\bar{3}m$ symmetry. (c) Schematic illustration of the ABCBA stacking in a HPL model with DPOSS domains shown in blue. (d) GISAXS pattern of the thin film in (a) after further annealing at 160 °C for 11 h. The Miller indexes in the GISAXS pattern are based on (e) the 2D orthorhombic lattice of the c-HEX structure. (f) Schematic illustration of cylindrical packing in the c-HEX model with DPOSS domains shown in blue.

surfactant system, with an asymmetric phase diagram similar to diblock copolymers.[38] Interestingly, giant surfactants exhibit unconventional spheroidal micelle phases, such as the dodecagonal quasicrystal structure and the Frank-Kasper A15 and σ-phase, driven by their multitailed molecular geometry.[39] Recently, we demonstrated tunable and complex phase behaviors of giant surfactants in thin films by balancing the interaction parameter and the molecular topologies with the surface field and geometrical confinement.[40]

The rich self-assembly behavior and highly tunable structures of giant surfactants make them ideal candidates for further investigations on the thickness-dependent phase stability in thin films. The study on phase formation, stability, and transitions, especially the bicontinuous DG phase, in thin films lays the foundation toward developing bottom-up fabrication techniques and other potential applications.

RESULTS AND DISCUSSION

Double Gyroid Phase in the Bulk. The self-assembly behavior of a series of BPOSS-PS_n-DPOSS samples (BPOSS and DPOSS stand for butyl- and hydroxyl-functionalized POSS cages, respectively) with various molecular weights of PS has been studied in the bulk state.[41] A sequence of phase transitions from LAM → DG → HEX → BCC was observed for BPOSS-PS_n-DPOSS by systematically increasing the molecular weight of the central PS from 1.2K to 12K Da (which roughly corresponds to n = 12 to 120). Similar molecular conjugates with two different nanoparticles telechelically linked to a polymer chain have also been evaluated by molecular simulations.[42] Among this series of samples, BPOSS-PS_{28}-DPOSS (Figure 1) was found to form a DG structure. In this contribution, we select this giant surfactant sample and are interested in the stability of the 3D bicontinuous structure under thin film confinement.

First, the DG structure of BPOSS-PS_{28}-DPOSS in the bulk was identified via synchrotron SAXS and bright field (BF) TEM images of the microtomed samples. The SAXS pattern (Figure 2a) clearly shows the characteristic diffraction peaks of a DG lattice with a q-value ratio of $\sqrt{6}$, $\sqrt{8}$, $\sqrt{14}$, $\sqrt{16}$, $\sqrt{20}$, $\sqrt{22}$, $\sqrt{24}$, $\sqrt{26}$, $\sqrt{30}$, and $\sqrt{38}$. The cubic lattice parameter was determined to be a = 21.8 nm, and the corresponding crystallographic details are summarized in Table S1. The BF TEM images shown in Figures 2b, 2c, and 2d represent the bicontinuous structure along the ⟨001⟩, ⟨111⟩, and ⟨110⟩ projection directions of the cubic lattice, respectively. The spot-to-spot distance ($d_{220,DG}$) in Figure 2b is measured as 7.7 nm, indicating a DG cubic lattice with a = 21.8 nm, which matches the observation of the location of the (211) reflection in the

DOI: 10.1021/acs.macromol.7b01598
Macromolecules 2017, 50, 7282−7290

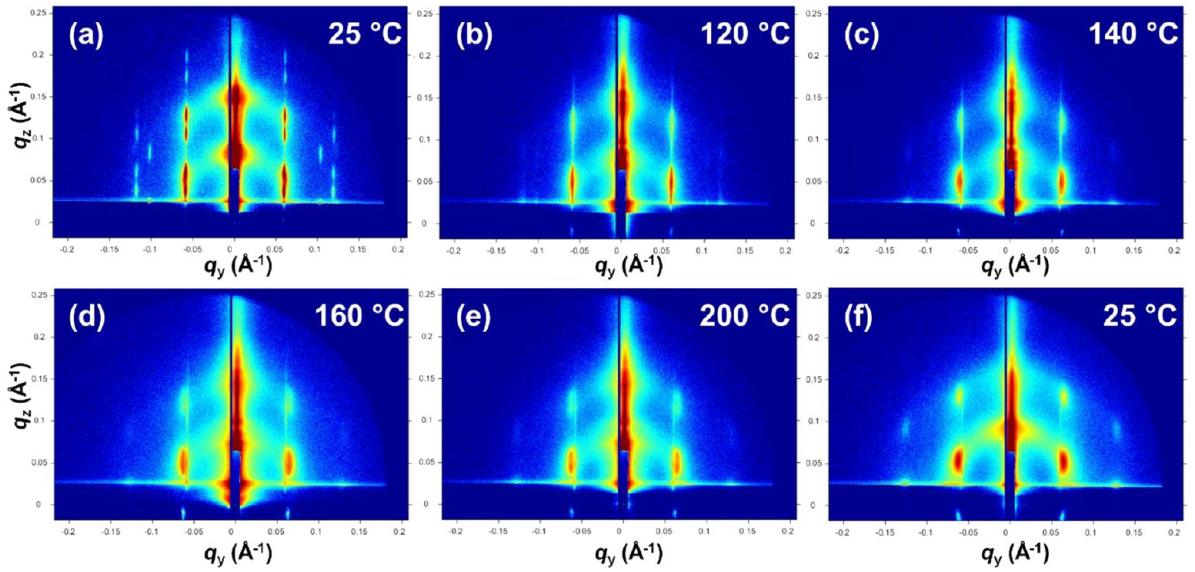

Figure 4. *In situ* GISAXS patterns at an incident angle of 0.20° of a 65 nm thick ($7L_0$) film upon heating and subsequent cooling to room temperature. The patterns were collected at (a) 25, (b) 120, (c) 140, (d) 160, (e) 200, and (f) 25 °C. Each pattern was collected after holding at the specific temperature more than 10 min.

SAXS powder pattern. Using density measurements, the volume fractions of DPOSS, BPOSS, and PS in BPOSS-PS_{28}-DPOSS are determined as 0.22, 0.19, and 0.59, respectively.[41] In our previous study of BPOSS-PS-DPOSS with PS midblocks of various molecular weights, we found that BPOSS cages and PS chains are miscible except in the LAM phase, where the flat geometry facilitates the crystallization of BPOSS cages. Therefore, the matrix (majority domain) of this DG structure is a mixed BPOSS and PS domain, while the two interwoven minority networks, each having a volume fraction of 11%, are solely composed of the hydrophilic DPOSS cages.

To confirm the assignment of the phase composition of the DG phase, the structure factors with varied scattering factors of the two domains were calculated based on the level surface model of DG to compare with the experimental data.[43] The calculation shows that the case with major volume fraction (Φ_1) equal to 0.78 and the minor volume fraction (Φ_2) equal to 0.22 matches much better with the experimental data than the case of $\Phi_1 = 0.59$ (pure PS) with $\Phi_2 = 0.41$ (one network of BPOSS, one network of DPOSS), further indicating that the DPOSS cages comprises the two minority networks and that the matrix consists of a mixture of PS chains and BPOSS cages (Supporting Information). The combined TEM images and SAXS structure factor calculations also exclude the possibility that BPOSS-PS_{28}-DPOSS forms alternating or core−shell DG structures.[44−46] Note that the identified relative volume fractions of this DG structure significantly deviates from the typical volume fractions region where a normal DG phase appears in linear diblock copolymers (~64:36). This is attributed to the conformational rigidity of DPOSS cages, which tends to increase the "effective chain cross-section area" at the interfaces and thus results in shifted phase boundaries and a low volume fraction of DPOSS ($\Phi_{DPOSS} = 0.22$) for the double network component.[39] It is also worth noting that in addition to the DG phase a minor amount of the HEX phase is observed as faint additional reflections in the 1D SAXS pattern (Figure S1). Indeed, the HEX phase is expected to appear on the bulk sample surface, which is observed for thick films. According to our detailed analysis of scattered intensity (structure factor section in the Supporting Information) of both the DG and HEX phases, the mechanically extruded bulk sample after annealing at 120 °C has approximately 84% DG and 16% HEX by volume. The coexistence of the DG and HEX phases will be further discussed in the section on thick films.

Thickness-Dependent Phase Transition in Thin Films. The grazing-incidence SAXS (GISAXS) pattern of a 138 nm thick film of BPOSS-PS_{28}-DPOSS after annealing at 120 °C for 4 days is shown in Figure 3a. The strong reflections along the q_z direction at $q_y = 0$ Å^{-1} indicate a layered structure, and the additional reflections along the q_z direction at $q_y \neq 0$ Å^{-1} imply lateral structural correlations between and within the layers. The pattern is consistent with a HPL structure with lattice parameters of $a = b = 12.4$ nm, $c = 27.4$ nm, $\alpha = \beta = 90°$, and $\gamma = 120°$ with space group $R\bar{3}m$, No. 166 (Figure 3b). For the pattern simulation, the motifs are arranged in the Wyckoff position of 3*a* with coordinates of [0, 0, 0], [1/3, 2/3, 1/3], and [2/3, 1/3, 2/3] in the hexagonal lattice (contoured in the black solid lines). The calculated transmitted (red circles) and reflected (white squares) signals are overlaid to the right-hand side of the GISAXS pattern, which match well with the experimental GISAXS pattern (Figure 3a). The HPL structure is schematically illustrated in Figure 3c with DPOSS perforated layers in blue and the BPOSS/PS matrix omitted for clarity. The stacking scheme of the perforated layers in the HPL structure is determined to be ABCBA trigonal stacking based on the matching of the simulated and the experimental reflections in the GISAXS pattern, while the simulated scattering signals for ABA and ACA hexagonal stacking are different from the experimental data (Figure S2).[20]

When the same thin film sample was further annealed at 160 °C for 11 h, the corresponding GISAXS pattern is different from that of the HPL structure (Figure 3d). Qualitatively, this pattern indicates a structure composed of cylinders with the cylindrical axis perpendicular to the thin film normal. A closer examination, however, reveals that the pattern cannot be simply fitted with a 2D hexagonal lattice. Notably, the cylinder layer spacing along the film normal direction is compressed by 14.2%, resulting in a *compressed* HEX structure (c-HEX) that

DOI: 10.1021/acs.macromol.7b01598
Macromolecules 2017, 50, 7282−7290

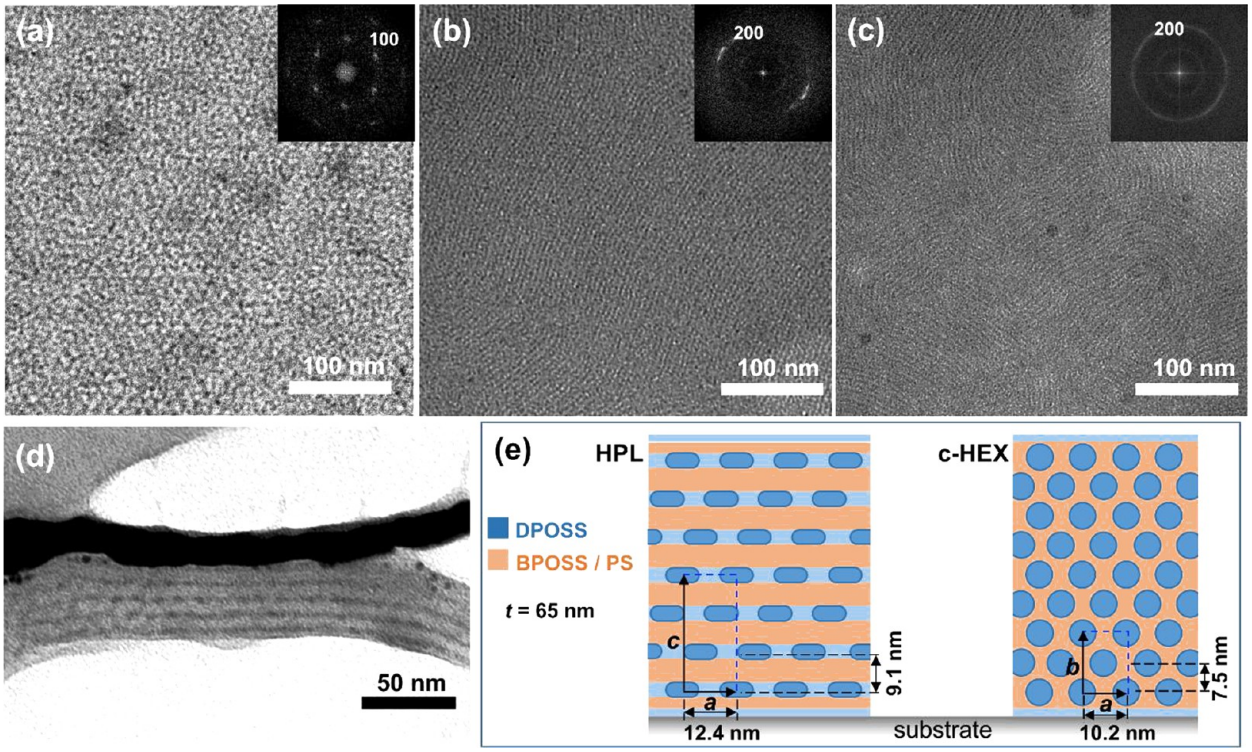

Figure 5. A set of BF TEM images of a 65 nm thick ($7L_0$) film after different thermal treatments. The plane-view images of the film after annealing at (a) 120, (b) 128, and (c) 150 °C for 2 days. The insets represent the corresponding FFT images. (d) Cross-sectional view of the film after annealing at 120 °C for 2 days. The black strip represents the Au layer deposited on the air/film interface. (e) Schematic illustration of the comparison between HPL and c-HEX structures in the cross-sectional view.

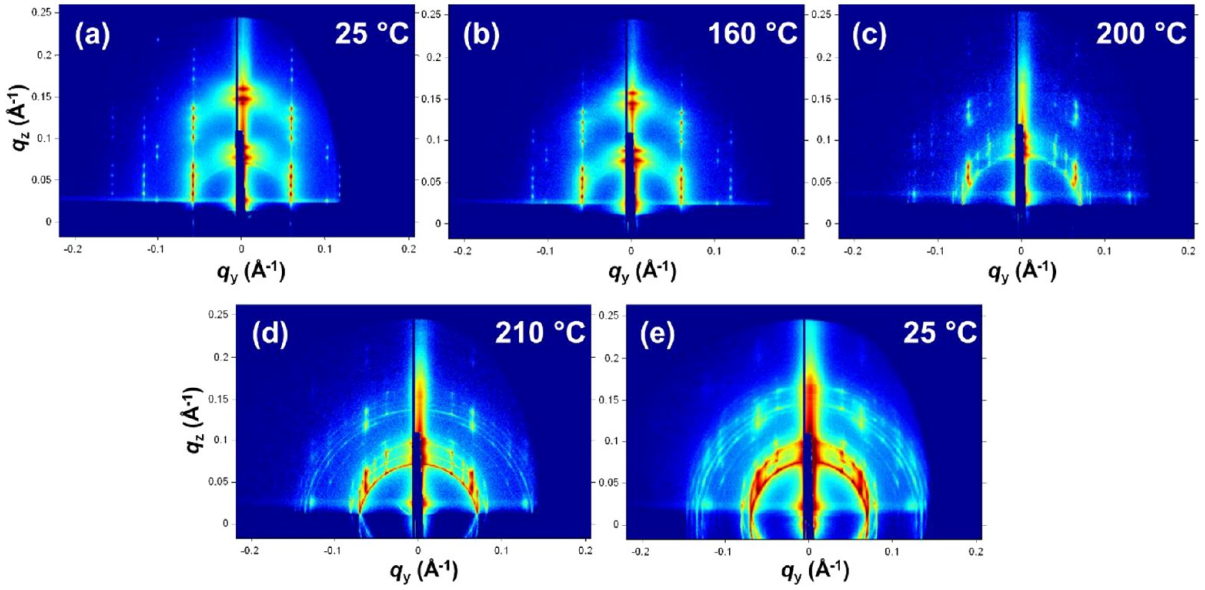

Figure 6. *In situ* GISAXS patterns at an incident angle of 0.20° of a 300 nm thick ($33L_0$) film upon heating and subsequent cooling to room temperature. The patterns were collected at (a) 25, (b) 160, (c) 200, (d) 210, and (e) 25 °C. Each pattern was collected after maintaining the film at the specific temperature for more than 10 min.

can be described by a centered 2D orthorhombic lattice with a = 10.2 nm, b = 15.1 nm, and plane group $p2mm$ (Figure 3e). A simplified 3D illustration is shown in Figure 3f.

To understand the phase transition in thin films, GISAXS experiments were conducted on films with various thicknesses as a function of temperature at Beamline 8-ID-E of the Advanced Photon Source. From a set of GISAXS patterns of a 65 nm thick film recorded both upon heating and upon subsequent cooling to room temperature (Figure 4), it is observed that the pattern of a HPL structure transforms into the pattern of a HEX phase between 120 and 140 °C, suggesting a HPL → HEX phase transition upon heating. There is no further transition observed up to 200 °C, and the anisotropic thermal contraction of the HEX structure along the

DOI: 10.1021/acs.macromol.7b01598
Macromolecules 2017, 50, 7282−7290

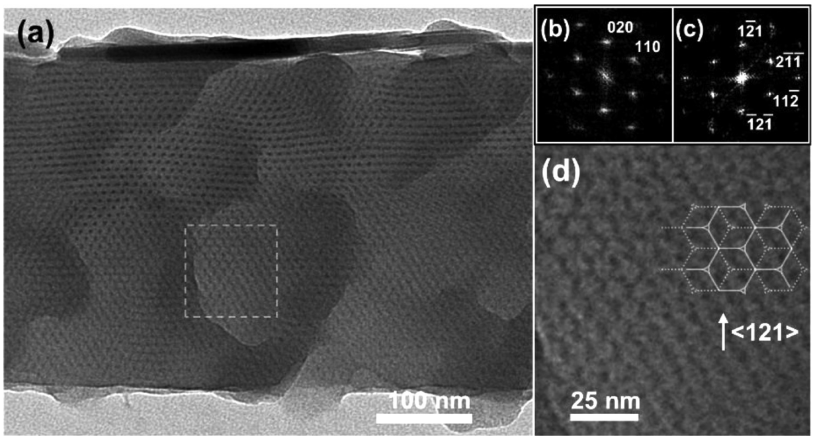

Figure 7. BF TEM images of a 300 nm thick ($33L_0$) film. (a) The cross-sectional view of the 300 nm thick film after the *in situ* GISAXS experiments at various temperatures. The black strip in (a) is the amorphous carbon layer deposited on the air/film interface, and the bottom of the film sample represents the film/substrate interface. (b) Corresponding FFT image of the upper part (c-HEX) and (c) the lower part (DG) of (a). (d) Magnified image of the outlined region in (a).

film normal direction during cooling back to room temperature creates the c-HEX structure. The assignments of the HEX at 200 °C and the c-HEX structures at 25 °C are confirmed by the pattern analysis (Figure S3). The change from the HEX lattice to the c-HEX lattice is attributed to the small thickness shrinkage (~3 nm) during cooling, as revealed by the *in situ* reflectivity data (Figure S4). Overall, we observed an irreversible HPL → HEX phase transition from the 65 nm thick BPOSS-PS_{28}-DPOSS film, and the same phase behavior was also observed for a 138 nm thick film (summarized in Figure S5).

To confirm the phase we observed during *in situ* GISAXS measurements is a long-term stable phase, we examined a long-term-annealed (2 days) 65 nm thick film by TEM. When viewed along the film normal direction, the film after being annealed at 120 °C for 2 days shows the HPL structure (Figure 5a), and the corresponding fast Fourier transform (FFT) image in the inset clearly shows the 6-fold symmetry of the morphology. The cross-sectional view (Figure 5d) of the film reveals the perforated layered structure with DPOSS in dark and BPOSS/PS in gray after the selective OsO_4 staining of the hydroxyl groups on the DPOSS cages. The air/film interface is covered by a layer of hydrophilic DPOSS, which is also observed for thicker films (Figure S6b). The distance between two neighboring perforated DPOSS layers is about 9 nm, which coincides with the layer periodicity of the HPL structure determined from the GISAXS pattern. In contrast, thin films annealed at 128 and 150 °C (Figures 5b and 5c) show the c-HEX structure in the plane-view images. This set of TEM data clearly confirms the observed phase behavior in GISAXS experiments. A schematic comparison of the cross sections between the HPL and the c-HEX microdomain structures is illustrated in Figure 5e. The periodicity of {003} planes of the HPL structure is 9.1 nm, which is close to the {10} plane periodicity (i.e., 8.8 nm) of the HEX with a = 10.2 nm, indicating a likely epitaxial relationship with each other. However, due to the compression of c-HEX along its b-axis, the dimension between layers of cylinders (i.e., 7.5 nm) is smaller than the layer periodicity of the HPL phase (i.e., 9.1 nm). Considering the $\{003\}_{HPL}$ = 9.1 nm is the domain spacing (L_0) in the system, the 300, 138, and 65 nm thick films represent films having $33L_0$, $15L_0$, and $7L_0$ periods, respectively.

In contrast to the phase behavior in thin films with thickness less than 200 nm, films thicker than 200 nm exhibit a different phase transition upon heating. Figure 6 shows a series of *in situ* GISAXS patterns of a 300 nm thick ($33L_0$) film upon heating and subsequent cooling. The HPL structure in this thick film does not transform to the c-HEX but reorganizes to the DG phase at 200 °C (Figure 6c). Moreover, the subsequent cooling process does not bring back the HPL phase (Figure 6e), thus indicating an irreversible HPL → DG phase transition. By using the GIXSGUI software to fit the diffraction patterns, we can determine that the DG phase orients with its ⟨121⟩ direction perpendicular to the substrate, and that the lattice parameter of the DG phase is a = 21.8 nm, which coincides with the unit cell dimension of the bulk DG phase. The GISAXS pattern of the DG phase with the calculated allowed *Ia*3*d* reflection positions overlay is summarized in Figure S7a. The two different phase behaviors of HPL → c-HEX for thickness <200 nm and HPL → DG for thickness >200 nm demonstrate the unique thickness dependence of this bolaform-like giant surfactant.

Surface-Induced HPL Phase. To further investigate the thickness-dependent self-assembly phenomenon in thin films, the 300 nm thick ($33L_0$) film studied in the *in situ* GISAXS experiment was also observed by TEM. The cross-sectional view TEM image (Figure 7a) clearly shows the c-HEX structure in the vicinity of air/film interface with the DG structure developed in the bulk interior of the film. Because the TEM sample preparation involves peeling thin film samples from the substrate (see Experimental Section for details), the nanostructure in the vicinity of the substrate appears as DG. However, additional TEM images show the presence of c-HEX domain in the substrate interface (Figure S8); moreover, the substrate layer of c-HEX is usually thinner than at the air/film interface, indicating DPOSS prefers to contact air (lowest interfacial tension) and it is only slightly favorable at the silicon substrate. Figures 7b and 7c represent the corresponding FFT images of the c-HEX and DG structures shown in Figure 7a, respectively. The magnified image of the DG structure (Figure 7d) confirms the observation in GISAXS patterns that the ⟨121⟩ direction is perpendicular to the substrate and also reveals the expected epitaxial relationship between $\{121\}_{DG}$ and $\{10\}_{HEX}$,[47] where $d_{121,DG}$ = 8.9 nm and $d_{10,HEX}$ = 8.8 nm (observed at 200 and 210 °C). A careful analysis of the GISAXS pattern of Figure 6e confirms a coexistence of DG/HEX at high temperature

DOI: 10.1021/acs.macromol.7b01598
Macromolecules 2017, 50, 7282−7290

(Figure 6c,d) and DG/c-HEX after cooling down to room temperature (Figure 6e). The local maximum intensities of the reflections on the quadrant provides the dimensions of a = 10.2 nm and b = 16.5 nm for the c-HEX structure (Figure S7b). According to these observations, the origin of the c-HEX should be that the layered HPL structure close to an interface prefers transforming to the c-HEX structure after thermal treatment up to 210 °C. Although there are some variations for the overall thickness of the c-HEX near-surface region from the observation of TEM, the average thickness of c-HEX domain from both the air and silicon interface is about 200 nm (Figure 7a and Figure S8). This suggests the surface effect penetrates into the film up to around 200 nm, consistent with the switchover point from the HPL → c-HEX transition to the HPL → DG transition at around 200 nm thickness. In addition, the degree of compression of the c-HEX phase is not uniform. The compression along the b-axis of the c-HEX phase varies; for example, the compression is 14.2%, 7.0%, and 6.2% in Figure 3d (160 °C), Figure 4f (25 °C), and Figure S7b, respectively. These results indicate that the c-HEX phase is a kinetically trapped structure, which depends on the thermal history and sample preparation, and that the noncompressed HEX structure with *p6mm* symmetry is the equilibrium phase for regions closed to film surfaces.

CONCLUSION

The DG-forming BPOSS-PS_{28}-DPOSS sample exhibits film thickness-dependent phase transitions upon heating. The surface-induced HPL phase dominates the morphology for thin films for annealing at 120 °C. The irreversible HPL → c-HEX phase transition takes place at around 130 °C for films with thickness less than 200 nm. In contrast, the films with thickness >200 nm exhibit the irreversible HPL → DG phase transition at 200 °C. Because surface fields tend to suppress density variations in the direction parallel to the surfaces and therefore stabilize layered structures, these results indicate that the metastable HPL phase is stabilized by the thin film geometry and the surface field. The HPL phase in a relative thin film (thickness $<20L_0$) cannot transform to the bulk equilibrium DG phase because the surface field still dominates the free energy upon heating. The energy barrier of HPL → HEX is lowered by the surface field so that it becomes a kinetically favorable pathway, which follows the epitaxial relationship between $\{003\}_{HPL}$ and $\{10\}_{HEX}$. Once the film is many tens of unit cells thick (thickness $>20L_0$), the bulk equilibrium morphology dominates the interior of the film because the "surface field" effect does not extend to far into the bulk, resulting a HPL → c-HEX phase transition in the vicinity of interfaces and a HPL → DG phase transition in the midportion of the films with epitaxial relationship between $\{003\}_{HPL}$ and $\{121\}_{DG}$. These results demonstrate that the transition pathway that a soft material adopts depends on the film thickness, which is essential to understand for many thin film applications, such as thin film ceramic coatings and nanoporous separation membranes.

EXPERIMENTAL SECTION

Material and Thin Film Preparation. The synthetic route of BPOSS-PS_{28}-DPOSS is briefly described in the Supporting Information (Scheme S1). Thin film samples of BPOSS-PS_{28}-DPOSS were prepared by spin-coating (Specialty Coating System, spin-coater model P6700) of a tetrahydrofuran (THF) solution of BPOSS-PS_{28}-DPOSS onto silicon wafers. The silicon wafers were pretreated with piranha solution (concentrated H_2SO_4/30% H_2O_2 = 3:1 (v/v)) at 80 °C for 30 min, followed by rinsing with deionized water and drying with nitrogen flow. The thickness of the films was controlled by the solvent concentration and the applied spin speed. Specifically, spin-coating of a 1.0 wt % solution at 2000 rpm, a 2.0 wt % solution at 1000 rpm, a 5.0 wt % solution at 2000 rpm, and a 5.0 wt % solution at 1000 rpm for 60 s generates films with thicknesses of 65, 138, 193, and 300 nm, respectively.

Small-Angle X-ray Scattering (SAXS). The bulk sample for SAXS was prepared by mechanical extrusion (0.7 mm in diameter) followed by annealing at 120 °C for 2 h. The 1D SAXS pattern was collected in the beamline 12-ID-B at the Advanced Photon Source. The experiment was conducted under vacuum at room temperature. Beamline 12-ID-B operates at the energy of 14 keV, and the scattering signals were collected by a Pilatus 2M area detector. The beam size is 200 (H) × 10 (V) μm^2, and the sample−detector distance is 1157.5 mm.

Grazing Incidence Small-Angle X-ray Scattering (GISAXS). The high-resolution grazing-incidence X-ray scattering experiments was conducted in the beamline 8-ID-E at the Advanced Photon Source.[48] The GISAXS patterns were collected at the incident angle of 0.2° under vacuum to maximize the scattering signal for the entire film. Beamline 8-ID-E operates at the energy of 7.35 keV, and the scattering signals were collected by a Pilatus 1M-F area detector. The GISAXS patterns were analyzed by the GIXSGUI package.[49] The red circles and white open squares in the indexed GISAXS patterns represent the transmitted and reflected signals, respectively. The beam size is 100 (H) × 50 (V) μm^2, and the sample−detector distance is 1473.62 mm. *In situ* heating and cooling GISAXS measurements were conducted under vacuum on a thermal stage with a upper limit of 220 °C at 10 °C/min heating and cooling rates.

Reflectivity. Reflectivity measurements were conducted prior to GISAXS measurements with the same setup. The reflectivity data were collected in the range of 2θ = 0.2°−2.2°. The thicknesses of thin film samples reported in this work were determined by reflectivity.

Ellipsometry. The thickness of the films was quantified using spectroscopic ellipsometry (VASE, J.A. Woollam). The spectroscopic data were collected in the wavelength region of 300−1000 nm at three angles: 65°, 70°, and 75°. The model with a Cauchy film on the silicon substrate was applied to approximate the film thickness via the WVASE32 software. The thickness information obtained from ellipsometry was used to screen the sample preparation before the GISAXS and reflectivity experiments in the synchrotron beamline.

Transmission Electron Microscopy (TEM). BF TEM images were collected using a JEOL-1230 microscope with an accelerating voltage of 120 kV. For the plane-view images, a layer of amorphous carbon layer (~20 nm) was first deposited on the thin film sample. A drop of poly(acrylic acid) (PAA) 25% aqueous solution was then applied on the sample and dried. The sample (film/carbon layer/PAA) was then peeled off the silicon wafer with the aid of a razor blade. After dissolving the PAA in water by placing the sample with the PAA face down on the water surface, the film sample with carbon layer was then be picked up by a copper grid. For cross-sectional view images, a layer of Au or amorphous carbon layer (~30 nm) was deposited on the thin films. The thin film samples were transferred from the silicon wafer to the water surface by PAA and then picked up by a piece of cured epoxy (Epofix cold-setting embedding resin, #1232, EMS). Thin slices (80 nm thick) of the sample using a microtome (Leica EM UC7) at room temperature were then transferred to copper grids. All the samples were subjected to OsO_4 staining for 16 h prior to the TEM examination for preferential staining of the hydroxyl groups on the DPOSS.

ASSOCIATED CONTENT

Supporting Information

The Supporting Information is available free of charge on the ACS Publications website at DOI: 10.1021/acs.macromol.7b01598.

DOI: 10.1021/acs.macromol.7b01598
Macromolecules 2017, 50, 7282−7290

Synthetic route of the BPOSS-PS_{28}-DPOSS giant surfactant, crystallographic information on the double gyroid structure of BPOSS-PS_{28}-DPOSS in bulk, analysis of 1D SAXS powder pattern for BPOSS-PS_{28}-DPOSS, and phase behavior of thin films (PDF)

AUTHOR INFORMATION

Corresponding Authors

*E-mail scheng@uakron.edu (S.Z.D.C.).
*E-mail elt@rice.edu (E.L.T.).

ORCID

Stephen Z. D. Cheng: 0000-0003-1448-0546

Notes

The authors declare no competing financial interest.

ACKNOWLEDGMENTS

This work was supported by the National Science Foundation (DMR-1408872). This research used resources of the Advanced Photon Source, a U.S. Department of Energy (DOE) Office of Science User Facility operated for the DOE Office of Science by Argonne National Laboratory under Contract DE-AC02-06CH11357.

ABBREVIATIONS

POSS, polyhedral oligomeric silsesquioxane; BPOSS, butyl-functionalized POSS; DPOSS, hydroxyl-functionalized POSS; PS, polystyrene; LAM, lamellae; DG, double gyroid; HEX, hexagonally packed cylinders; c-HEX, compressed hexagonally packed cylinders; BCC, body-centered-cubic packed spheres; HPL, hexagonal perforated layer; BF, bright field; FFT, fast Fourier transform; GISAXS, grazing-incidence small-angle X-ray scattering; L_0, domain spacing.

REFERENCES

(1) Bita, I.; Yang, J. K. W.; Jung, Y. S.; Ross, C. A.; Thomas, E. L.; Berggren, K. K. Graphoepitaxy of self-assembled block copolymers on two-dimensional periodic patterned templates. *Science* **2008**, *321*, 939−943.

(2) Cheng, J. Y.; Ross, C. A.; Smith, H. I.; Thomas, E. L. Templated self-assembly of block copolymers: Top-down helps bottom-up. *Adv. Mater.* **2006**, *18*, 2505−2521.

(3) Bates, C. M.; Maher, M. J.; Janes, D. W.; Ellison, C. J.; Willson, C. G. Block Copolymer Lithography. *Macromolecules* **2014**, *47*, 2−12.

(4) Hsueh, H.-Y.; Ho, R.-M. Bicontinuous Ceramics with High Surface Area from Block Copolymer Templates. *Langmuir* **2012**, *28*, 8518−8529.

(5) Edrington, A. C.; Urbas, A. M.; DeRege, P.; Chen, C. X.; Swager, T. M.; Hadjichristidis, N.; Xenidou, M.; Fetters, L. J.; Joannopoulos, J. D.; Fink, Y.; Thomas, E. L. Polymer-based photonic crystals. *Adv. Mater.* **2001**, *13*, 421−425.

(6) Luzzati, V.; Spegt, P. A. Polymorphism of Lipids. *Nature* **1967**, *215*, 701−704.

(7) Thomas, E. L.; Alward, D. B.; Kinning, D. J.; Martin, D. C.; Handlin, D. L.; Fetters, L. J. Ordered Bicontinuous Double-Diamond Structure of Star Block Copolymers - a New Equilibrium Microdomain Morphology. *Macromolecules* **1986**, *19*, 2197−2202.

(8) Hajduk, D. A.; Harper, P. E.; Gruner, S. M.; Honeker, C. C.; Kim, G.; Thomas, E. L.; Fetters, L. J. The Gyroid - a New Equilibrium Morphology in Weakly Segregated Diblock Copolymers. *Macromolecules* **1994**, *27*, 4063−4075.

(9) Schulz, M. F.; Bates, F. S.; Almdal, K.; Mortensen, K. Epitaxial Relationship for Hexagonal-to-Cubic Phase-Transition in a Block-Copolymer Mixture. *Phys. Rev. Lett.* **1994**, *73*, 86−89.

(10) Matsen, M. W.; Bates, F. S. Block copolymer microstructures in the intermediate-segregation regime. *J. Chem. Phys.* **1997**, *106*, 2436−2448.

(11) Matsen, M. W.; Schick, M. Stable and Unstable Phases of a Linear Multiblock Copolymer Melt. *Macromolecules* **1994**, *27*, 7157−7163.

(12) Ahn, J. H.; Zin, W. C. Structure of shear-induced perforated layer phase in styrene-isoprene diblock copolymer melts. *Macromolecules* **2000**, *33*, 641−644.

(13) Thomas, E. L.; Anderson, D. M.; Henkee, C. S.; Hoffman, D. Periodic Area-Minimizing Surfaces in Block Copolymers. *Nature* **1988**, *334*, 598−601.

(14) Almdal, K.; Koppi, K. A.; Bates, F. S.; Mortensen, K. Multiple Ordered Phases in a Block Copolymer Melt. *Macromolecules* **1992**, *25*, 1743−1751.

(15) Disko, M. M.; Liang, K. S.; Behal, S. K.; Roe, R. J.; Jeon, K. J. Catenoid-Lamellar Phase in Blends of Styrene-Butadiene Diblock Copolymer and Homopolymer. *Macromolecules* **1993**, *26*, 2983−2986.

(16) Hamley, I. W.; Koppi, K. A.; Rosedale, J. H.; Bates, F. S.; Almdal, K.; Mortensen, K. Hexagonal mesophases between lamellae and cylinders in a diblock copolymer melt. *Macromolecules* **1993**, *26*, 5959−5970.

(17) Spontak, R. J.; Smith, S. D.; Ashraf, A. Dependence of the Obdd Morphology on Diblock Copolymer Molecular-Weight in Copolymer Homopolymer Blends. *Macromolecules* **1993**, *26*, 956−962.

(18) Förster, S.; Khandpur, A. K.; Zhao, J.; Bates, F. S.; Hamley, I. W.; Ryan, A. J.; Bras, W. Complex Phase-Behavior of Polyisoprene-Polystyrene Diblock Copolymers near the Order-Disorder Transition. *Macromolecules* **1994**, *27*, 6922−6935.

(19) Vigild, M. E.; Almdal, K.; Mortensen, K.; Hamley, I. W.; Fairclough, J. P. A.; Ryan, A. J. Transformations to and from the gyroid phase in a diblock copolymer. *Macromolecules* **1998**, *31*, 5702−5716.

(20) Zhu, L.; Huang, P.; Cheng, S. Z. D.; Ge, Q.; Quirk, R. P.; Thomas, E. L.; Lotz, B.; Wittmann, J.-C.; Hsiao, B. S.; Yeh, F.; Liu, L. Dislocation-Controlled Perforated Layer Phase in a PEO- b-PS Diblock Copolymer. *Phys. Rev. Lett.* **2001**, *86*, 6030−6033.

(21) Zhu, L.; Huang, P.; Chen, W. Y.; Ge, Q.; Quirk, R. P.; Cheng, S. Z. D.; Thomas, E. L.; Lotz, B.; Hsiao, B. S.; Yeh, F.; Liu, L. Nanotailored Crystalline Morphology in Hexagonally Perforated Layers of a Self-Assembled PS-b-PEO Diblock Copolymer. *Macromolecules* **2002**, *35*, 3553−3562.

(22) Zhu, L.; Huang, P.; Chen, W. Y.; Weng, X.; Cheng, S. Z. D.; Ge, Q.; Quirk, R. P.; Senador, T.; Shaw, M. T.; Thomas, E. L.; Lotz, B.; Hsiao, B. S.; Yeh, F.; Liu, L. Plastic Deformation" Mechanism and Phase Transformation in a Shear-Induced Metastable Hexagonally Perforated Layer Phase of a Polystyrene-b-poly(ethylene oxide) Diblock Copolymer. *Macromolecules* **2003**, *36*, 3180−3188.

(23) Laradji, M.; Shi, A. C.; Desai, R. C.; Noolandi, J. Stability of ordered phases in weakly segregated diblock copolymer systems. *Phys. Rev. Lett.* **1997**, *78*, 2577−2580.

(24) Olmsted, P. D.; Milner, S. T. Strong segregation theory of bicontinuous phases in block copolymers. *Macromolecules* **1998**, *31*, 4011−4022.

(25) Qi, S. Y.; Wang, Z. G. On the nature of the perforated layer phase in undiluted diblock copolymers. *Macromolecules* **1997**, *30*, 4491−4497.

(26) Jin, S.; Yoon, J.; Heo, K.; Park, H.-W.; Kim, J.; Kim, K.-W.; Shin, T. J.; Chang, T.; Ree, M. Detailed analysis of gyroid structures in diblock copolymer thin films with synchrotron grazing-incidence X-ray scattering. *J. Appl. Crystallogr.* **2007**, *40*, 950−958.

(27) Lee, B.; Park, I.; Yoon, J.; Park, S.; Kim, J.; Kim, K.-W.; Chang, T.; Ree, M. Structural Analysis of Block Copolymer Thin Films with Grazing Incidence Small-Angle X-Ray Scattering. *Macromolecules* **2005**, *38*, 4311−4323.

(28) Park, I.; Lee, B.; Ryu, J.; Im, K.; Yoon, J.; Ree, M.; Chang, T. Epitaxial Phase Transition of Polystyrene-b-Polyisoprene from Hexagonally Perforated Layer to Gyroid Phase in Thin Film. *Macromolecules* **2005**, *38*, 10532−10536.

DOI: 10.1021/acs.macromol.7b01598
Macromolecules 2017, 50, 7282−7290

(29) Shin, C.; Ryu, D. Y.; Huh, J.; Kim, J. H.; Kim, K. W. Order-to-Order Transitions of Block Copolymer in Film Geometry. *Macromolecules* **2009**, *42*, 2157−2160.
(30) Jung, J.; Park, H. W.; Lee, S.; Lee, H.; Chang, T.; Matsunaga, K.; Jinnai, H. Effect of Film Thickness on the Phase Behaviors of Diblock Copolymer Thin Film. *ACS Nano* **2010**, *4*, 3109−3116.
(31) Yang, G.; Tang, P.; Yang, Y. L.; Cabral, J. T. Self-Assembly of AB Diblock Copolymers under Confinement into Topographically Patterned Surfaces. *J. Phys. Chem. B* **2009**, *113*, 14052−14061.
(32) Huinink, H. P.; van Dijk, M. A.; Brokken-Zijp, J. C. M.; Sevink, G. J. A. Surface-induced transitions in thin films of asymmetric diblock copolymers. *Macromolecules* **2001**, *34*, 5325−5330.
(33) Knoll, A.; Horvat, A.; Lyakhova, K. S.; Krausch, G.; Sevink, G. J. A.; Zvelindovsky, A. V.; Magerle, R. Phase behavior in thin films of cylinder-forming block copolymers. *Phys. Rev. Lett.* **2002**, *89*, 035501.
(34) Bai, W.; Yager, K. G.; Ross, C. A. In Situ Characterization of the Self-Assembly of a Polystyrene−Polydimethylsiloxane Block Copolymer during Solvent Vapor Annealing. *Macromolecules* **2015**, *48*, 8574−8584.
(35) Yin, Y.; Sun, P.; Jiang, R.; Li, B.; Chen, T.; Jin, Q.; Ding, D.; Shi, A.-C. Simulated annealing study of asymmetric diblock copolymer thin films. *J. Chem. Phys.* **2006**, *124* (18), 184708.
(36) Li, W.; Liu, M.; Qiu, F.; Shi, A.-C. Phase Diagram of Diblock Copolymers Confined in Thin Films. *J. Phys. Chem. B* **2013**, *117*, 5280−5288.
(37) Zhang, W.-B.; Yu, X.; Wang, C.-L.; Sun, H.-J.; Hsieh, I. F.; Li, Y.; Dong, X.-H.; Yue, K.; Van Horn, R.; Cheng, S. Z. D. Molecular Nanoparticles Are Unique Elements for Macromolecular Science: From "Nanoatoms" to Giant Molecules. *Macromolecules* **2014**, *47*, 1221−1239.
(38) Yu, X.; Yue, K.; Hsieh, I.-F.; Li, Y.; Dong, X.-H.; Liu, C.; Xin, Y.; Wang, H.-F.; Shi, A.-C.; Newkome, G. R.; Ho, R.-M.; Chen, E.-Q.; Zhang, W.-B.; Cheng, S. Z. D. Giant surfactants provide a versatile platform for sub-10-nm nanostructure engineering. *Proc. Natl. Acad. Sci. U. S. A.* **2013**, *110*, 10078−10083.
(39) Yue, K.; Huang, M.; Marson, R.; He, J.; Huang, J.; Zhou, Z.; Wang, J.; Liu, C.; Yan, X.; Wu, K.; Guo, Z.; Liu, H.; Zhang, W.; Ni, P.; Wesdemiotis, C.; Zhang, W.-B.; Glotzer, S. C.; Cheng, S. Z. D. Geometry Induced Sequence of Nanoscale Frank-Kasper and Quasicrystal Mesophases in Giant Surfactants. *Proc. Natl. Acad. Sci. U. S. A.* **2016**, *113*, 14195−14200.
(40) Hsu, C.-H.; Dong, X.-H.; Lin, Z.; Ni, B.; Lu, P.; Jiang, Z.; Tian, D.; Shi, A.-C.; Thomas, E. L.; Cheng, S. Z. D. Tunable Affinity and Molecular Architecture Lead to Diverse Self-Assembled Supramolecular Structures in Thin Films. *ACS Nano* **2016**, *10*, 919−929.
(41) Wu, K.; Huang, M. J.; Yue, K.; Liu, C.; Lin, Z. W.; Liu, H.; Zhang, W.; Hsu, C. H.; Shi, A. C.; Zhang, W. B.; Cheng, S. Z. D. Asymmetric Giant "Bolaform-like" Surfactants: Precise Synthesis, Phase Diagram, and Crystallization-Induced Phase Separation. *Macromolecules* **2014**, *47*, 4622−4633.
(42) Marson, R. L.; Phillips, C. L.; Anderson, J. A.; Glotzer, S. C. Phase Behavior and Complex Crystal Structures of Self-Assembled Tethered Nanoparticle Telechelics. *Nano Lett.* **2014**, *14*, 2071−2078.
(43) Wohlgemuth, M.; Yufa, N.; Hoffman, J.; Thomas, L. E. Triply periodic bicontinuous cubic microdomain morphologies by symmetries. *Macromolecules* **2001**, *34*, 6083−6089.
(44) Goldacker, T.; Abetz, V. Core-shell cylinders and core-shell gyroid morphologies via blending of lamellar ABC triblock and BC diblock copolymers. *Macromolecules* **1999**, *32*, 5165−5167.
(45) Shefelbine, T. A.; Vigild, M. E.; Matsen, M. W.; Hajduk, D. A.; Hillmyer, M. A.; Cussler, E. L.; Bates, F. S. Core-shell gyroid morphology in a poly(isoprene-*block*-styrene-*block*-dimethylsiloxane) triblock copolymer. *J. Am. Chem. Soc.* **1999**, *121*, 8457−8465.
(46) Epps, T. H., III; Cochran, E. W.; Hardy, C. M.; Bailey, T. S.; Waletzko, R. S.; Bates, F. S. Network phases in ABC triblock copolymers. *Macromolecules* **2004**, *37*, 7085−7088.
(47) Vigild, M. E.; Almdal, K.; Mortensen, K.; Hamley, I. W.; Fairclough, J. P. A.; Ryan, A. J. Transformations to and from the Gyroid Phase in a Diblock Copolymer. *Macromolecules* **1998**, *31*, 5702−5716.
(48) Jiang, Z.; Li, X.; Strzalka, J.; Sprung, M.; Sun, T.; Sandy, A. R.; Narayanan, S.; Lee, D. R.; Wang, J. The Dedicated High-Resolution Grazing-Incidence X-Ray Scattering Beamline 8-ID-E at The Advanced Photon Source. *J. Synchrotron Radiat.* **2012**, *19*, 627−636.
(49) Jiang, Z. GIXSGUI: A MATLAB Toolbox for Grazing-Incidence X-Ray Scattering Data Visualization and Reduction, and Indexing of Buried Three-Dimensional Periodic Nanostructured Films. *J. Appl. Crystallogr.* **2015**, *48*, 917−926.

DOI: 10.1021/acs.macromol.7b01598
Macromolecules 2017, 50, 7282−7290